Journal of Peptide Science
J. Pept. Sci. 2008; **14**: 184–191
Published online 26 November 2007 in Wiley InterScience (www.interscience.wiley.com). DOI: 10.1002/psc.973

JOURNAL OF PEPTIDE SCIENCE

Electroconductive and photocurrent generation properties of self-assembled monolayers formed by functionalized, conformationally-constrained peptides on gold electrodes‡

EMANUELA GATTO,[a] LORENZO STELLA,[a] FERNANDO FORMAGGIO,[b] CLAUDIO TONIOLO,[b] LEANDRO LORENZELLI[c] and MARIANO VENANZI[a]*

[a] Department of Chemical Sciences and Technologies and Centro NAST, University of Rome Tor Vergata, 00133 Rome, Italy
[b] Institute of Biomolecular Chemistry, Padova Unit, CNR, Department of Chemistry, University of Padova, 35131 Padova, Italy
[c] Bruno Kessler Foundation-IRST, 38050 Trento, Italy

Received 27 June 2007; Revised 28 September 2007; Accepted 10 October 2007

Abstract: The electroconductive properties and photocurrent generation capabilities of self-assembled monolayers formed by conformationally-constrained hexapeptides were studied by cyclic voltammetry, chronoamperometry, and photocurrent generation experiments. Lipoic acid was covalently linked to the *N*-terminus of the peptides investigated to exploit the high affinity of the disulfide group to the gold substrates. Smart functionalization of the peptide scaffold with a redox-active (TOAC) or a photosensitizer (Trp) amino acid allowed us to study the efficiency of peptide-based self-assembled monolayers to mediate electron transfer and photoinduced electron transfer processes on gold substrates. Interdigitated microelectrodes have shown higher film stability under photoexcitation, lower dark currents, and higher sensitivity with respect to standard gold electrodes. Copyright © 2007 European Peptide Society and John Wiley & Sons, Ltd.

Supplementary electronic material for this paper is available in Wiley InterScience at http://www.interscience.wiley.com/jpages/1075-2617/suppmat/

Keywords: conformationally-constrained peptides; electroconductive properties; interdigitated gold microelectrodes; peptide self-assembled monolayers; photocurrent generation

INTRODUCTION

New bio-hybrid devices based on the integration of biological molecules and metal substrates are currently actively explored for potential applications in the areas of molecular recognition, biological sensing, and molecular electronics [1–3]. Biological materials such as DNA, peptides, and proteins have been investigated as potential elements of molecular electronic devices, principally for their ability to self-assemble and to attain structurally ordered conformations. In particular, their self-assembling properties allow to precisely build up nanostructures that are not currently achievable with conventional silicon-based technologies (*bottom-up* approach) [4].

Over the past few years, electrochemical studies and photocurrent generation experiments on peptides immobilized on surfaces have become a viable alternative for studying electron transfer (ET) processes [5]. Suitably functionalized peptides have been covalently linked to gold surfaces making use of the strong Au–S interaction (≈40 kcal mol^{-1}), forming highly ordered self-assembled monolayers (SAMs) [6,7]. SAMs formed by peptides functionalized with redox-active groups have shown peculiar electronic conduction properties in terms of long-range and directional ET [8,9]. The introduction of conformationally-constrained residues in the peptide chain [10,11], allowed to control the peptide secondary structure, modulating the separation between the active group and the gold surface.

In this work, we present experimental results concerning two peptides specifically designed for electrochemical and photocurrent generation studies. The primary structure of the first, an hexapeptide denoted in the following as SSA4TA, comprises three α-aminoisobutyric acid (Aib) residues, a non-coded α-amino acid characterized by two methyl groups on the C$^{\alpha}$ atom, two alanine residues and a 2,2,6,6-tetramethylpiperidine-1-oxyl-4-amino-4-carboxylic acid (TOAC) residue located at position 5 (Figure 1). TOAC is a redox-active amino acid [12], widely used as a probe in ESR experiments [13,14] or as a quencher of aromatic molecules in fluorescence studies [15,16]. X-ray photoelectron spectroscopy (XPS), FT-IR absorption, and ESR measurements have shown that this peptide is able to form stable SAMs on gold substrates [17].

*Correspondence to: Mariano Venanzi, Department of Chemical Sciences and Technologies, University of Rome Tor Vergata, via della Ricerca Scientifica, 00133 Rome, Italy; e-mail: venanzi@uniroma2.it
‡This article is part of the Special Issue of the Journal of Peptide Science entitled "Peptides in Nanotechnology".

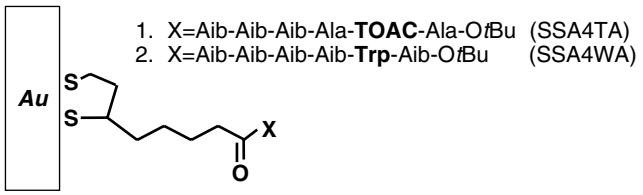

Figure 1 Primary structures (and acronyms) of the lipoyl peptides investigated (O*t*Bu, *tert*-butoxy). The Au–S linkage has been also schematically represented.

A second oligopeptide, denoted in the following as SSA4WA, was specifically synthesized for photocurrent generation studies. This peptide was shown to be able to form a densely-packed SAM on gold surfaces, with interesting growth dynamics and mobility properties [6,18]. The primary structure of SSA4WA comprises five Aib residues and a Trp unit located at position 5 (Figure 1). The latter amino acid is an intrinsic fluorescent species with high absorption properties in the near-UV region. SSA4WA has been covalently linked to different gold electrodes to study the electron conduction properties of the resulting SAM and its ability to generate photocurrent upon UV irradiation.

Both peptides were functionalized at the *N*-terminus with a lipoyl group to exploit the high Au–S affinity for covalently linking the peptides on gold surfaces. It has been shown that *N*-terminally bound peptides give rise to more densely-packed SAMs on gold than those obtained from *C*-terminally bound peptides [8], owing to additional polarization effects arising from the electric macrodipole associated to an helically ordered peptide. The high content of the conformationally restricted Aib residues [10] in both peptides is responsible for the rigid helical structure adopted by SSA4TA and SSA4WA, despite the shortness of their main chain [6,15].

MATERIALS AND METHODS

Materials

(*S,R*)-Lipoyl-(Aib)$_3$-(*S*)-Ala-TOAC-(*S*)-Ala-O*t*Bu (SSA4TA) was synthesized by reacting (*S,R*)-α-lipoic acid (Fluka, Büchs, Switzerland) with H-(Aib)$_3$-(S)-Ala-TOAC-(S)-Ala-O*t*Bu in methylene chloride solution [17]. The TOAC residue was incorporated using the *N*-ethyl,*N*′-(3-dimethylaminopropyl) carbodiimide (EDC)/1-hydroxy-7-aza-benzotriazole (HOAt) approach [19], while the Aib residues were inserted via the symmetrical anhydride method [20]. The sequence following TOAC was built up using fluoren-9-ylmethoxycarbonyl N^{α}-protection. (*S,R*)-Lipoyl-(Aib)$_4$-(*S*)-Trp-Aib-O*t*Bu (SSA4WA) was prepared by reacting (*S,R*)-α-lipoic acid with H-(Aib)$_4$-(*S*)-Trp-Aib-O*t*Bu in methylene chloride solution using the EDC/HOAt C-activation method [6].

Spectrograde solvents were exclusively used (Carlo Erba, Italy). Water was distilled and passed through a Milli-Q purification system. Other chemicals, triethanolamine – TEOA (Fluka), potassium chloride (Carlo Erba), sodium sulphate (Carlo Erba), potassium ferricyanide (Aldrich), methylviologen (Aldrich), and undecanethiol (Aldrich) were all of reagent grade quality and used without further purification.

Gold interdigitated microelectrodes (IDEs) were prepared by evaporating a 200 nm gold layer on a 100 nm thick layer of Si_3N_4. IDEs were arranged in a series of parallel electrodes, each one 20 μm wide and positioned at a distance of 20 μm, the length of each finger being 1 mm. IDEs were etched for 15 min in a piraña solution (2 : 1 sulphuric acid : H_2O_2, v/v) before immersion in a peptide solution for SAM preparation, then rinsed with bidistilled water and ethanol.

Preparation of Self-Assembled Peptide Thin Films

SAM-coated electrodes were prepared by immersing a gold electrode into a 1 mM ethanol solution of the peptide or undecanethiol ($C_{11}H_{24}S$) in a N_2 atmosphere. After 18 h of immersion, the electrode was carefully rinsed with ethanol (to remove physically adsorbed peptides from the SAM) and dried under a gentle argon flow.

Methods. Cyclic voltammograms (CVs) were obtained by using a PG-310 potentiostat (HEKA Elektronik, Lambrecht, Germany) at room temperature. A standard three electrodes configuration was used with a SAM-coated gold electrode as the working electrode and a platinum wire as the auxiliary electrode. In the case of photocurrent generation experiments and blocking experiments with ferricyanide, the reference electrode was Ag/AgCl, while for the electroactive SAM in ethanol solution the reference electrode was a saturated calomel electrode (SCE) with a junction. $K_3Fe(CN)_6$ 0.5 mM in 1 M KCl was used as the electroactive component in the blocking experiment. For the latter measurements the sweep rate was set at 50 mV s^{-1}. CVs of the electroactive peptide SAM were obtained in a 0.2 M $NaClO_4$ ethanolic solution, using a SAM-coated gold electrode as the working electrode. Cyclic voltammetry experiments were carried out at sweep rates ranging from 25 to 250 mV s^{-1}. Chronoamperometry experiments were carried out at room temperature using the three-electrode set-up described above. The potential was changed symmetrically with respect to the standard redox potential: in the case of a standard redox potential of 0.6 V and an overpotential of 0.04 V, the potential was applied from 0.56 to 0.64 V for the TOAC oxidation and then returned back to 0.56 for the $TOAC^+$ reduction.

Photocurrent measurements were carried out at room temperature using the three-electrode set-up described above. The supporting electrolyte was Na_2SO_4 (0.1 M). TEOA was used as a sacrificial electron donor at 50 mM concentration. The SAM-modified electrodes were irradiated with a Xe lamp (150 W) equipped with a monochromator. The photocurrents generated from the SAM-coated electrodes were detected by the voltammetric analyzer described above. The intensity of the incident light was evaluated by azobenzene actinometry [21].

RESULTS AND DISCUSSION

Electrochemical Studies on SSA4TA

SSA4TA has been covalently linked to a gold electrode for studying the electron conduction properties of the resulting SAM.

DOI: 10.1002/psc

Cyclic voltammetry experiments. A typical CV of the SSA4TA SAM is shown in Figure 2, where reversible redox peaks at potential values characteristic of the TOAC group (0.596 V *vs* SCE) are readily observed.

At sufficiently slow scan rates, typically 0.1 V s^{-1} or slower, reversible conditions are attained and ideal CVs are obtained, in that the observed peak splittings (ΔE_p) and peak half-widths are both very small (0 ± 4 and 90 mV, respectively) [22,23]. This result indicates that all the redox centers are in a rather uniform environment, as that provided by an ordered film. On the contrary, a disordered electroactive monolayer should have exhibited a set of formal potentials generated by locally varying dielectric constant with significant broadening of the peaks observed.

CVs of the SSA4TA SAM performed at different sweep rates showed that the oxidative peak current linearly increases with the scan rate (Supplementary Information), indicating that the observed CV peaks arise from surface-bound TOAC groups [24]. In agreement with these considerations, sweep-rate dependent cyclic voltammetry experiments performed on the simple amino acid derivative Boc-TOAC-OH (Boc, *tert*-butoxycarbonyl) in solution showed that the oxidation peak linearly depends on the square root of the scan rate. In this case, a standard redox potential very similar to that measured in the peptide SAM (0.60 V *vs* SCE) was obtained, confirming the view that the interfacial potential drop of adsorbed molecules is quite small.

The electrode surface coverage of the peptide SAM can be obtained from cyclic voltammetry experiments by integrating the oxidative peak after subtraction of the background current (Figure 2):

$$I_p(\upsilon) = \frac{N \cdot n^2 \cdot F^2}{4 \cdot R \cdot T}\upsilon$$

In the above equation I_p is the anodic (cathodic) peak current, υ the voltage scan rate, N the number of redox-active sites on the surface, n the number of electrons transferred, F the Faraday constant, R the universal gas constant, and T the temperature. From the slope of I_p versus υ ($n = 1$) we estimate a surface coverage of 14.4×10^{-11} mol cm^{-2}. This value agrees very well with that theoretically obtained by assuming closely packed helical peptide chains, i.e. 16.6×10^{-11} mol cm^{-2} [25].

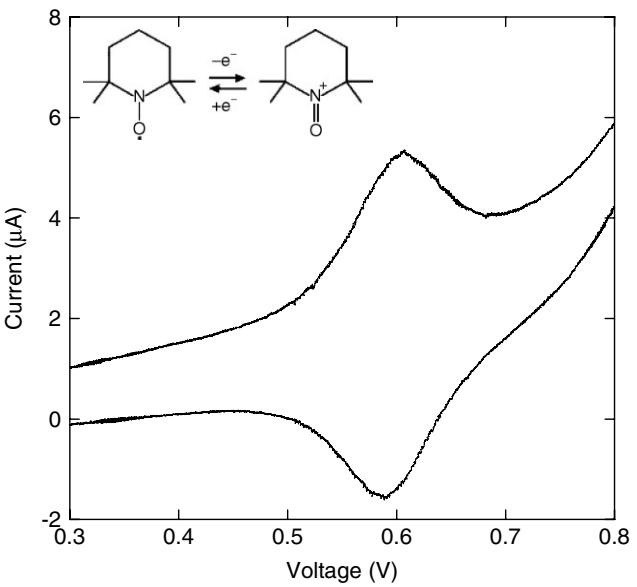

Figure 2 Typical cyclic voltammogram of a gold electrode modified with a SSA4TA SAM at 25 °C (scan rate 0.025 V s^{-1}). Inset: electrochemical reaction of the TOAC group.

Chronoamperometry experiments. The *along-the-molecule* distance between the TOAC group and the gold surface can be roughly estimated to be 17 Å. This value is obtained by summing the molecular length of the peptide backbone in a rigid 3_{10}-helix arrangement (≈2.0 Å rise per residue) [10] to the lipoyl chain in an all-*trans* conformation (7.3 Å) [26]. At this distance, a super-exchange mechanism, which is characterized by an exponential dependence of the ET rate constant on the distance and by a strong dependence on the overpotential, most likely takes place.

Chronoamperometry experiments were carried out for characterizing the ET process from TOAC to the gold electrode through the peptide SAM. In interfacial ET reactions between surface-bound redox groups and metal electrodes, the current I is expected to decay exponentially with time, according to the equation:

$$I = I_o e^{-k_{ET} \cdot t}$$

where I_0 is the current at $t = 0$ and k_{ET} is the ET rate constant. Experimental $I - t$ curves for SSA4TA in the 2–200 μs time region were analyzed by this equation to determine k_{ET} at different positive overpotentials, i.e. the difference between the applied potential and the standard redox potential of TOAC (a typical $I - t$ decay of SSA4TA is reported as Supplementary Information).

The ET rate constants for the TOAC oxidation at different positive overpotentials and those for the $TOAC^+$ reduction at different negative overpotentials (Tafel plot) are shown in Figure 3. A strong dependence of the ET rate constants on the applied potential was observed, similar to that found in the case of SAMs composed of alkanethiols or other sulfur-terminated compounds [23,27]. This finding confirms the view that a super-exchange mechanism takes place in the short peptide investigated.

The standard rate constant for ET, i.e. the rate constant at the standard redox potential, was determined by extrapolating the data in Figure 3 to a null overpotential. As a result, k_{ET} from TOAC to gold was found to be 9.2 s^{-1}, while for the back ET from gold to $TOAC^+$ the standard rate constant was 9.3 s^{-1}.

DOI: 10.1002/psc

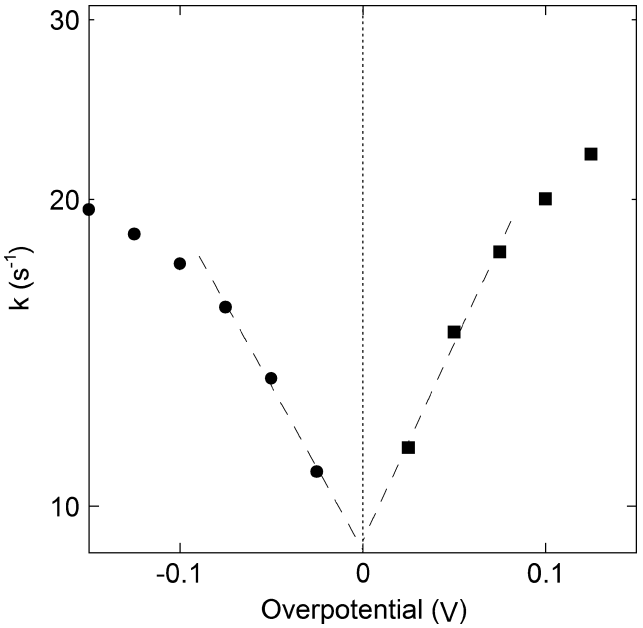

Figure 3 Dependence of the ET rate constant (k_{ET}) on the applied overpotential (V) for TOAC oxidation (filled squares) and $TOAC^+$ reduction (filled circles) at the gold electrode through the SSA4TA SAM.

Interestingly, the Tafel plot shows a marked asymmetry of the k_{ET} values versus overpotential curves for oxidative and reductive conditions. This effect is probably ascribable to the electrostatic field generated by the electric macrodipole associated with the helical peptide chain. At positive overpotentials electrons are transferred from TOAC to the gold electrode (k_a), i.e. from the *C*-terminus to the *N*-terminus, while for negative overpotentials ET occurs in the opposite direction (k_c), i.e. from the *N*-terminus to the *C*-terminus.

As the electric macrodipole is directed from the *C*-terminus (δ^-) to the *N*-terminus (δ^+), k_a at a given overpotential is expected to be higher than k_c. From the data reported in Figure 3, k_a/k_c is 1.19 ± 0.05.

This value is definitely smaller than that observed in α-helical peptides [7], suggesting that the electric field effect on the ET process in 3_{10}-helical peptides is less important, probably because of the distortion of the hydrogen-bond network with respect to the helical axis. This result is fully consistent with that obtained by time-resolved fluorescence measurements for photoinduced ET in 3_{10}-helical peptides in solution [28].

The reported electrochemical experiments indicate that the electroactive groups are embedded in a rather homogeneous environment, which suggests the formation of an ordered peptide film. From previously reported FT-IR reflectance spectroscopy measurements on the same peptide [17], it was possible to determine the orientation of the peptide helical axis with respect to the normal to the surface, with the hypothesis of an homogeneous orientation of the peptide helices. This value was found to be about 40°, in good agreement with literature values for vertically-oriented peptide SAMs [7,25]. From XPS measurements the film thickness was estimated to be 15 ± 2 Å [17]. Assuming a chain length of 22.4 Å for SSA4TA, it is possible to calculate the tilt angle, which was found to be about 48°. The good agreement between the two values of the tilt angles, obtained from independent experiments and molecular modeling, supports the view of an almost homogeneous SAM, vertically oriented with respect to the gold surface and quite densely packed.

Photocurrent Generation Experiments on SSA4WA

Despite the superior electron conductive properties of peptide spacers with respect to saturated hydrocarbon chains [29,30], photoinduced properties have been investigated much more extensively using alkanethiol SAMs [31,32] rather than peptide-based SAMs [8,33]. SSA4WA has been covalently linked to a gold electrode or to an interdigitated gold microelectrode for studying the photocurrent generation properties of the resulting SAM.

Photocurrent Generation by a SSA4WA SAM

The electronic current generated upon photoirradiation of the SSA4WA SAM on a gold electrode was investigated in the presence of an electron donor, such as TEOA. The photocurrents measured during repeated 30 s long on–off cycles of photoexcitation at different wavelengths are reported in Figure 4, where anodic signals almost instantaneously triggered by photoexcitation, can be clearly observed. The mechanism of anodic photocurrent generation by the peptide SAM is schematically presented in Figure 5. When the peptide layer is irradiated in the 260–320 nm UV range, the photoexcited Trp gives rise to an ET process from its singlet excited state to the surface Fermi level of the Au electrode. Subsequently, TEOA transfers an electron to the indole radical cation, and then the oxidized TEOA diffuses to the auxiliary electrode, taking an electron and giving rise to a net anodic electronic current.

The action spectrum of the SSA4WA SAM shows that the modified gold electrode has a photocurrent signal at the Trp absorption wavelengths larger than that of the bare gold electrode, emphasizing the role of Trp as a photosensitizer (Supplementary Information).

To investigate the ability of the peptide SAM to mediate the ET process from TEOA to gold, the dependence of the efficiency of anodic photocurrent generation on the applied electric potential was analyzed at the Trp maximum absorption wavelength ($\lambda_{max} = 280$ nm). For the peptide-modified gold electrode, a decrease in the anodic photocurrent with an increase of the negative bias to the working electrode was observed measuring a null photocurrent at a given characteristic potential (zero-current potential). A voltage negative bias reduces

DOI: 10.1002/psc

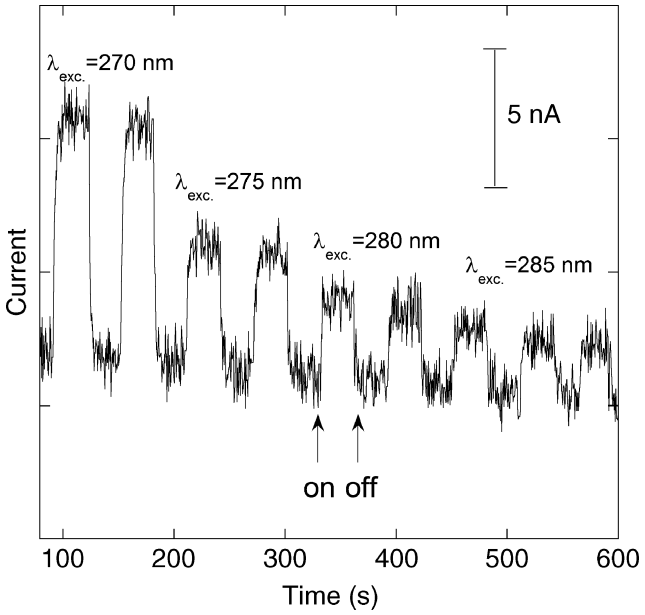

Figure 4 Time course of the photocurrent generated by a SSA4WA SAM in an aqueous TEOA solution at 0 V, upon photoirradiation at different wavelengths (room temperature).

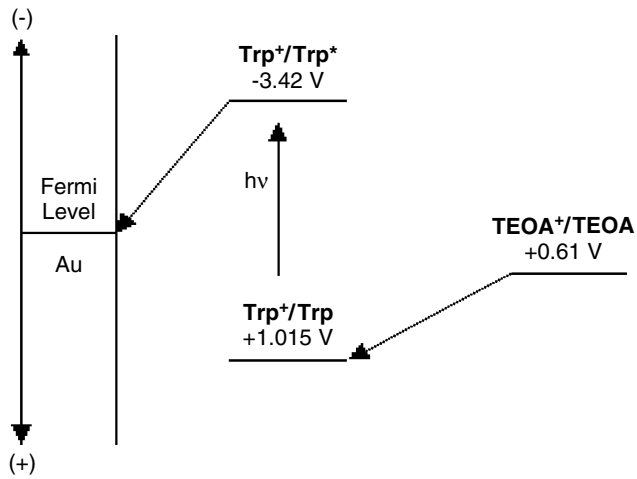

Figure 5 Energy diagram for anodic photocurrent generation in the presence of TEOA.

the energy gap between the oxidation potential of the excited Trp group and the gold Fermi level, resulting in a decrease of the anodic photocurrent. Notably, the anodic photocurrent changes to a cathodic photocurrent by applying a negative bias larger than the zero-current potential. It was suggested that, in this case, an electron acceptor group (H^+) in solution may accept an electron from the photoexcited Trp group to generate a cathodic photocurrent [8]. At the zero-current potential, cathodic and anodic photocurrents cancel each other out, apparently leading to a no current state. Interestingly, the SSA4WA SAM shows a negative zero-current potential value (−0.05 V). This value is most likely determined by the negative potential around the indole group generated by the helix dipole. The negative shift of the zero-current potential results in a larger driving force for photocurrent generation, accelerating the ET from the indole group to the gold surface. The expected potential shift induced by the dipole moment of the peptide helix (ϕ) can be calculated by the equation:

$$\phi = \frac{m \cdot n_a \cos\gamma}{\varepsilon_0 \varepsilon_m (1 + 9\alpha n_a^{3/2})}$$

where m, n_a, γ, ε_0, ε_m and α represent the helix dipole moment, the number of peptide molecules per unit area, the tilt angle of the helix axis from the surface normal, the vacuum dielectric permittivity, the relative dielectric constant of the monolayer, and the polarizability of the peptide molecule, respectively [34]. However, the potential generated by the helix dipole is reduced by the charge transfer from gold to the peptide layer associated to the partial ionic character of the Au^+S^- linkage [26]. On the contrary, peptides covalently linked to a gold surface at the *C*-terminus show a positive potential shift with respect to the potential measured for an alkanethiol SAM. By irradiation in the far-UV region ($\lambda_{exc} < 250$ nm), an anodic photocurrent was also measured for a bare gold electrode in contact with a TEOA solution. Photoelectrochemical studies on gold electrodes showed that anodic photocurrents can be ascribed to the presence of a thin oxide layer on the gold surface, in which Au_2O_3, having a fairly high absorption coefficient in the UV region [35], predominates. In addition, direct photoelectric effects on gold (the gold work function is 5.1 eV, corresponding to 243 nm) and TEOA absorbance (leading to $TEOA^* \rightarrow$ Au electron transfer) may contribute to the high photocurrent signal below 250 nm.

Photocurrent Generation by a Peptide SAM on Interdigitated Array Microelectrodes

Interdigitated array microelectrodes (IDEs) allowed us to perform cyclic voltammetry experiments with a better signal-to-noise ratio, because this type of electrodes can afford charge transport under steady-state conditions with much higher sensitivity and lower background dark current than standard gold electrodes [36,37]. IDEs were modified by a SAM formed from SSA4WA chemisorption on the gold surface. For comparison, IDEs modified by deposition of an undecanethiol SAM were also investigated. Cyclic voltammetry experiments confirmed that both SSA4WA and undecanethiol form densely-packed SAMs on the IDE, inhibiting almost completely the $K_3[Fe(CN)_6]$ electrolyte discharge (Supplementary Information). Photocurrent experiments in the Trp absorption region were performed on both the undecanethiol and the peptide-modified IDEs using TEOA as a sacrificial electron donor. In Figure 6 typical photocurrent intensities upon photoirradiation at

DOI: 10.1002/psc

280 nm of both alkanethiol- and peptide-modified IDEs are reported for comparison. The anodic photocurrent measured for the peptide-modified IDE is clearly seen, as opposed to the null response of the undecanethiol modified gold electrode.

The observed photocurrent intensity follows reversibly the on–off photoexcitation cycles, without apparent degradation of the anodic signal.

Photocurrent intensity versus applied potential voltage (P/V) experiments were also carried out at the Trp maximum absorption wavelength ($\lambda_{max} = 280$ nm). From the data reported in Figure 7, one may note the peculiar P/V dependence of the peptide-modified IDE, as opposed to the null P/V curve of the undecanethiol IDE. For the peptide-modified IDE, a decrease in the anodic photocurrent with an increase of the negative bias to the working electrode was observed, measuring a null photocurrent at a given, characteristic potential (zero-current potential = −0.150 V).

Importantly, the peptide SAM packing and homogeneity are not perturbed by photoirradiation, as shown by CV measurements on the same sample before and after the photocurrent experiment.

The incident photon-to-current efficiency (IPCE%) as a function of the excitation wavelength is reported in Figure 8 for the bare IDE, and for the IDE modified by deposition of the SSA4WA or the undecanethiol SAM. IPCE% is defined as the ratio of the electrons injected in the external circuit to the number of incident photons, and can be evaluated from the equation:

$$ICPE\% = 100 \cdot \frac{1240 \cdot i_{sc}}{I_{inc} \cdot \lambda}$$

where i_{sc} is the short circuit photocurrent (A cm^{-2}), I_{inc} the incident light intensity (W cm^{-2}), and λ the excitation wavelength (nm) [38]. As can be seen from the data reported in Figure 8, in the case of the bare IDE in an aqueous TEOA solution a cathodic photocurrent was observed. Vigorous cleaning of the IDE with piraña solution before each measurement leads us to rule out the hypothesis that such cathodic signal could arise from impurities absorbed on the gold surface [36]. Direct gold photoelectric events or photoinduced ET prompted by TEOA excitation are possibly responsible for such an effect.

On the contrary, the peptide-modified microelectrode, under the same experimental conditions, exhibits an intense anodic photocurrent signal (Figure 8). Figure 9 shows the ICPE% dependence on the applied potential voltage (P/V) at 240 nm for the bare gold microelectrode, and for IDEs modified by the peptide or by the undecanethiol SAM, respectively. The P/V curves indicate that the peptide SAM exhibits important rectifying

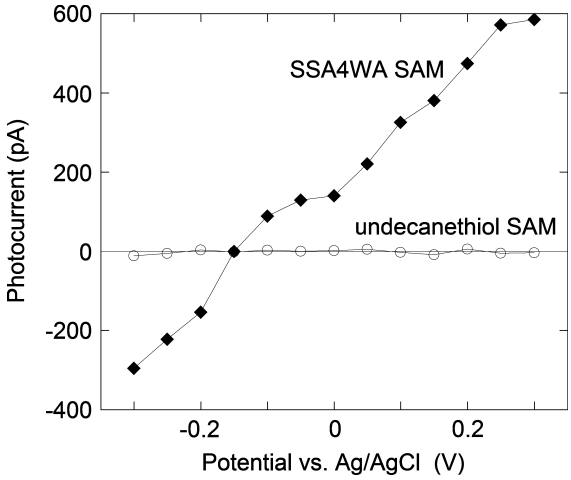

Figure 7 Photocurrent intensity of SAM-modified IDEs for different applied potentials (V) at $\lambda_{exc} = 280$ nm.

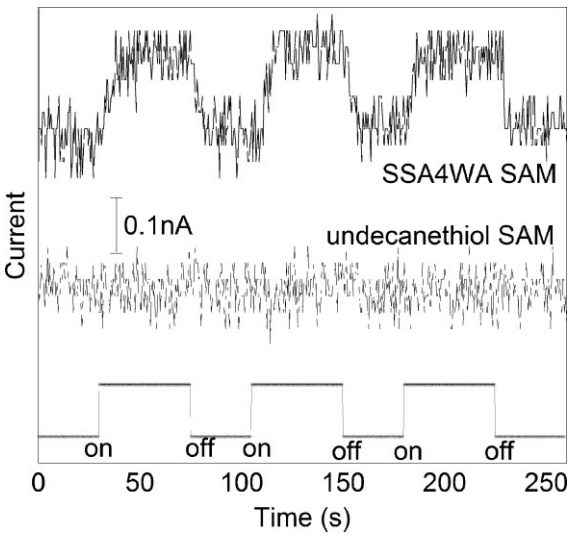

Figure 6 Time course of photocurrent intensity for IDEs modified by SSA4WA and undecanethiol SAMs. Applied potential versus Ag/AgCl: 0 V; $\lambda_{exc} = 280$ nm.

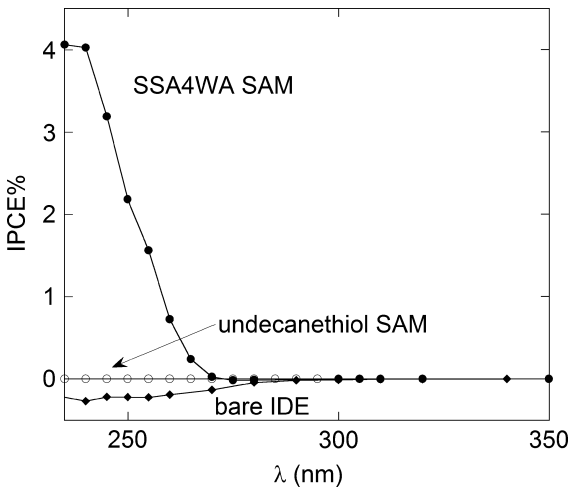

Figure 8 Photocurrent action spectrum of bare and SAM-modified interdigitated gold microelectrodes. Applied potential: 0 V versus Ag/AgCl, room temperature.

DOI: 10.1002/psc

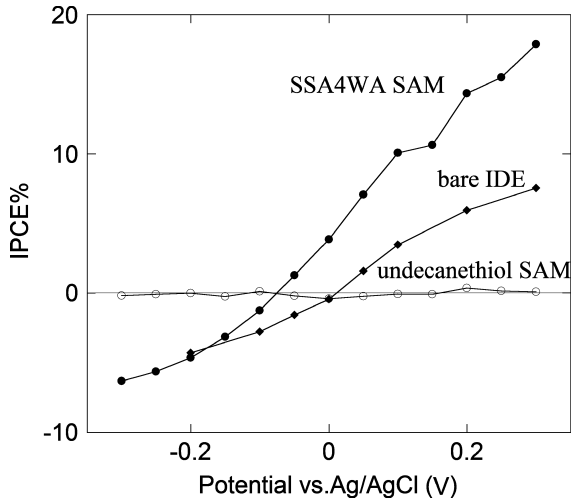

Figure 9 Incident photon-to-current efficiency (IPCE%) of bare and SAM-modified IDEs for different applied potentials (V) at $\lambda_{exc} = 240$ nm.

properties and contribute positively to the photocurrent generation efficiency also at this wavelength.

Interestingly, the zero photocurrent potential measured for the peptide-modified IDE is sensibly shifted to a more negative value with respect to the bare IDE. This effect is clearly ascribable to the electrostatic potential generated by the helix dipole, that stabilizes the $Au^{\delta+} \cdots S^{\delta-}$ bonding, making necessary higher negative potential to achieve cathodic photocurrent conditions. This finding emphasizes the role of the helix dipole effect in determining the electroconductive properties at the gold/SAM interface. Similar results were obtained at $\lambda_{exc} = 280$ nm.

CONCLUSIONS

Rectifying properties at the gold/peptide interface of an hexapeptide containing electroactive TOAC or Trp groups have been investigated by both electrochemical and photocurrent generation experiments. Cyclic voltammetry and chronoamperometry reveal that long-range ET occurs according to a super-exchange mechanism from TOAC to the gold surface through the peptide spacer. The peptide dipole moment does not affect the redox potential of the TOAC moiety, but it strongly influences the ET rate toward the gold substrate. The capability of a SAM composed of a helical peptide carrying a Trp group to sensitize anodic photocurrent by photoexcitation was investigated for a standard gold electrode and an interdigitated gold microelectrode. Cyclic voltammetry and photocurrent generation experiments indicate that the peptide forms a densely-packed and homogeneous SAM on the gold electrodes. Photocurrent experiments on IDEs demonstrated superior performances with respect to conventional gold electrodes in terms of response, sensitivity and reproducible results. Notably, applied potentials in the $-0.3 \div +0.3$ V range and repeated UV photoirradiation cycles did not damage the peptide SAM on IDE, confirming the SAM stability under the above experimental conditions.

These results show the good properties of helical peptides as mediators for long-range ET and their ability to control the direction of the current flow, paving the way for the development of molecular devices based on peptide molecular wires.

Supplementary Material

Supplementary electronic material for this paper is available in Wiley InterScience at: http://www.interscience.wiley.com/jpages/1075-2617/suppmat/

Acknowledgements

Financial support from PRIN2006 (MIUR, Italy) is gratefully acknowledged.

REFERENCES

1. Gooding JJ, Hibbert DB, Yang W. Electrochemical metal ion sensors. Exploiting amino acids and peptides as recognition elements. *Sensors* 2001; **1**: 75–90.
2. Nakamura C, Song SH, Chang SM, Sugimoto N, Miyake J. Quartz crystal microbalance sensor targeting low molecular weight compounds using oligopeptide binder and peptide-immobilized latex beads. *Anal. Chim. Acta* 2002; **469**: 183–188.
3. Niemeyer CM, Mirkin CA. *Nanobiotechnology*. Wiley-VCH: Weinheim, 2004.
4. Vijayender B, Bajpai RP, Bharadwaj LM. DNA electronics. *EMBO Rep.* 2003; **4**: 442–445.
5. Long YT, Abu-Irhayem E, Kraatz HB. Peptide electron transfer: more questions than answers. *Chem. – Eur. J.* 2005; **11**: 5186–5194.
6. Venanzi M, Pace G, Palleschi A, Stella L, Castrucci P, Scarselli M, De Crescenzi M, Formaggio F, Toniolo C, Marletta G. Densely-packed self-assembled monolayers on gold surfaces from a conformationally constrained helical hexapeptide. *Surf. Sci.* 2006; **600**: 409–416.
7. Sek S, Tolak A, Misicka A, Palys B, Bilewicz R. Asymmetry of electron transmission through monolayers of helical polyalanine adsorbed on gold surfaces. *J. Phys. Chem. B* 2005; **109**: 18433–18438.
8. Morita T, Kimura S, Kobayashi S, Imanishi Y. Photocurrent generation under a large dipole moment formed by self-assembled monolayers of helical peptides having an N-ethylcarbazolyl group. *J. Am. Chem. Soc.* 2000; **122**: 2850–2859.
9. Morita T, Kimura S. Long–range electron transfer over 4 nm governed by an inelastic hopping mechanism in self-assembled monolayers of helical peptides. *J. Am. Chem. Soc.* 2003; **125**: 8732–8733.
10. Toniolo C, Crisma M, Formaggio F, Peggion C. Control of peptide conformation by the Thorpe-Ingold effect (C^{α}-tetrasubstitution). *Biopolymers (Pept. Sci.)* 2001; **60**: 396–419.
11. Pispisa B, Mazzuca C, Palleschi A, Stella L, Venanzi M, Wakselman M, Mazaylerat JP, Rainaldi M, Formaggio F, Toniolo C. A combined spectroscopic and theoretical study of a series of conformationally restricted hexapeptides carrying a rigid binaphthylnitroxide donor-acceptor pair. *Chem. – Eur. J.* 2003; **9**: 4084–4093.

12. Toniolo C, Crisma M, Formaggio F. TOAC, a nitroxide spin-labeled, achiral C^{α}-tetrasubstituted α-amino acid, is an excellent tool in materials science and biochemistry. *Biopolymers (Pept. Sci.)* 1998; **47**: 153–158.
13. Hanson P, Martinez G, Millhauser G, Formaggio F, Crisma M, Toniolo C, Vita C. Distiguishing helix conformations in alanine-rich peptides using the unnatural amino acid TOAC and electron spin resonance. *J. Am. Chem. Soc.* 1996; **118**: 271–272.
14. Milov AD, Tsvetkov YD, Formaggio F, Crisma M, Toniolo C, Raap J. The secondary structure of a membrane-modifying peptide in a supramolecular assembly studied by PELDOR and CW-ESR spectroscopies. *J. Am. Chem. Soc.* 2001; **123**: 3784–3789.
15. Pispisa B, Palleschi A, Stella L, Venanzi M, Toniolo C. A nitroxide derivative as a probe for conformational studies of short linear peptides in solution. Spectroscopic and molecular mechanics investigations. *J. Phys. Chem. B* 1998; **102**: 7890–7898.
16. Venanzi M, Gatto E, Bocchinfuso G, Palleschi A, Stella L, Baldini C, Formaggio F, Toniolo C. Peptide folding dynamics: a time-resolved study from the nanosecond to the microsecond time regime. *J. Phys. Chem. B* 2006; **110**: 22834–22841.
17. Wen X, Linton RW, Formaggio F, Toniolo C, Samulski ET. Self-assembled monolayers of hexapeptides on gold: surface characterization and orientation distribution analysis. *J. Phys. Chem. A* 2004; **108**: 9673–9681.
18. Pace G, Venanzi M, Castrucci P, Scarselli M, De Crescenzi M, Palleschi A, Stella L, Formaggio F, Toniolo C, Marletta G. Static and dynamic features of a helical hexapeptide chemisorbed on a gold surface. *Mater. Sci. Eng., C* 2006; **26**: 918–923.
19. Carpino LA. 1-Hydroxy-7-aza-benzotriazole. An efficient peptide coupling additive. *J. Am. Chem. Soc.* 1993; **115**: 4397–4398.
20. McGahren WJ, Goodman M. Synthesis of peptide oxazolones and related compounds. *Tetrahedron* 1967; **23**: 2017–2030.
21. Kuhn JH, Braslavsky SE, Schmidt R. Chemical actinometry. *Pure Appl. Chem.* 1989; **61**: 187–211.
22. Brett CMA. *Electrochemistry Principles, Methods and Application*. Oxford University Press: Oxford, 1993.
23. Finklea HO, Hanshew DD. Electron-transfer kinetics in organized thiol monolayer with attached pentaammine(pyridine)ruthenium redox centers. *J. Am. Chem. Soc.* 1992; **114**: 3173–3181.
24. Watanabe J, Morita T, Kimura S. Effect of dipole moment, linkers, and chromophores at side chains on long-range electron transfer through helical peptides. *J. Phys. Chem. B* 2005; **109**: 14416–14425.
25. Fujita K, Bunjes N, Nakajima K, Hara M, Sasabe H, Knoll W. Macrodipole interactions of helical peptides in a self-assembled monolayer on gold substrates. *Langmuir* 1998; **14**: 6167–6172.
26. Miura Y, Kimura S, Kobayashi S, Iwamoto M, Imanishi Y, Umemura U. Negative surface potential produced by self-assembled monolayers of helix peptides oriented vertically to a surface. *Chem. Phys. Lett.* 1999; **315**: 1–6.
27. Sek S, Palys B, Bilewicz R. Contribution of intermolecular interactions to electron transfer through monolayers of alkanethiols containing amide groups. *J. Phys. Chem. B* 2002; **106**: 5907–5914.
28. Gatto E. *Conformationally constrained peptides as new nanomaterials for electrons and energy transfer*. PhD Dissertation, University of Rome Tor Vergata, 2007.
29. Sek S, Misicka A, Swiatek K, Maicka E. Conductance of α-helical peptides trapped within molecular junctions. *J. Phys. Chem. B* 2006; **110**: 19671–19677.
30. Sisido M, Hoshino S, Kusano H, Kuragaki M, Makino M, Sasaki H, Smith TA, Ghiggino KP. Distance dependence of photoinduced electron transfer along α-helical polypeptides. *J. Phys. Chem. B* 2001; **105**: 10407–10415.
31. Uosaki K, Kondo T, Zhang XQ, Yanagida M. Very efficient visible-light-induced uphill electron transfer at a self-assembled monolayer with a porphyrin-ferrocene-thiol linked molecule. *J. Am. Chem. Soc.* 1997; **119**: 8367–8368.
32. Imahori H, Norieda H, Ozawa S, Ushida K, Yamada H, Azuma T, Tamaki K, Sakata Y. Chain length effect on photocurrent from polymethylene-linked porphyrins in self-assembled monolayers. *Langmuir* 1998; **14**: 5335–5338.
33. Yasutomi S, Morita T, Imanishi Y, Kimura S. A molecular photodiode system that can switch photocurrent direction. *Science* 2004; **304**: 1944–1947.
34. Itoh E, Iwamoto M. Electronic density of state in metal/polyimide Langmuir-Blodgett film interface and its temperature dependence. *J. Appl. Phys.* 1997; **81**: 1790–1797.
35. Watanabe T, Gerischer H. Photoelectrochemical studies on gold electrodes with surface oxide layers. Part I. Photocurrent measurement in the visible region. *J. Electroanal. Chem.* 1981; **117**: 185–200.
36. Padeste C, Steiger B, Grubelnik A, Tiefenauer L. Molecular assembly of redox-conductive ferrocene-streptavidin conjugates towards bio-electrochemical devices. *Biosens. Bioelectron.* 2004; **20**: 545–552.
37. Stulik K, Amatore C, Holub K, Marecek V, Kutner W. Microelectrodes. Definition, characterization and applications. *Pure Appl. Chem.* 2000; **72**: 1483–1492.
38. Barazzouk S, Hotchandani S, Vinodgopal K, Kamat PV. Single-wall carbon nanotube films for photocurrent generation. A prompt response to visible-light irradiation. *J. Phys. Chem. B* 2004; **108**: 17015–17018.

DOI: 10.1002/psc